Establishing Climate Variability for Adaptation of Maritime Cultural and Natural Heritage to Climate Change in South Coast, Kenya

Wallace Njiiri[*1] Mugwima Njuguna[1] & Ephraim Wahome[2]

[1]*Centre for Urban Studies, Department of Landscape Architecture, Jomo Kenyatta University of Agriculture and Technology, Kenya (njiirikihiko@gmail.com)*

[1]*Centre for Urban Studies, Department of Landscape Architecture, Jomo Kenyatta University of Agriculture and Technology, Kenya(mugwima@sabs.ac.ke)*

[2]*Department of History and Archaeology, University of Nairobi, Kenya (ewahome@uonbi.ac.ke)*

**Corresponding author: njiirikihiko@gmail.com*

https://doi.org/10.62049/jkncu.v5i1.405

Abstract

Climate variability presents novel challenges to the conservation of maritime cultural and natural heritage. In the south Kenya coast, responses to extreme temperatures and sudden onset high rainfall worsen the condition of historic buildings and sacred landscapes, putting maritime communities at risk. To provide a baseline for prioritizing conservation planning initiatives, the paper sought to establish climate variability for the adaptation of maritime heritage to climate change. Between 1994 and 2024, average maximum and minimum temperatures rose by +1.6°C and +1.4°C, respectively. Linear regressions of average maximum and minimum temperatures showed high extremes of 32.10°C to 32.40°C and low extremes of 19.8°C to 20°C, respectively. The leptokurtic distribution showed a substantial chance of severe outcomes in average minimum and maximum temperatures in September and November, respectively. Over 30 years, the average maximum rainfall increased by 190mm with linear regressions indicating high extremes between 1500mm and 1600mm. The leptokurtic distribution revealed a substantial chance of extreme outcomes in average maximum rainfall in November. Average maximum and minimum temperatures for the final two years were considerably higher than the first two years; t (-5.2086, 1.0000) = 6.3138, P=0.0604) and t (--3.7226, 1.0000) = 6.3138, P=0.0835). However, average mean rainfall over the first two years was significantly lower than that over the latter two years t (-0.525, 1.000) = 6.3138, P =0.3460). Overall, unpredictability of short and long rainy seasons has increased during the last ten years compared to the previous twenty. Conservation planning is to consider physical stabilizations, shoreline consolidation, mangrove restoration, land use control, adjustments of setbacks and buffer zones to adapt maritime heritage to climate change.

Keywords: *Climate Variability, Maritime Heritage, Adaptation, Climate Change, South Kenya Coast*

Climate Variability and Maritime Heritage

Kenya's diverse maritime cultural heritage ranging from sea front mosques, forts, tombs, wells, coral stone and wattle-daub buildings as well as maritime natural heritage to include sacred forests, shrines and cultural landscapes are an essential part of the nation's identity and economic well-being. However, climate change amplifies the distribution of high temperatures and arid landscapes (Mulonga and Olago, 2023). In the south Kenya coast, responses to hotter drier weather (Lyon and Vigaud, 2017) have already been demonstrated by frequent drought cycles that result in significant landscape change (Maina et al., 2021).Warmer air and sea surface temperatures, driven by marine heat waves (Oliver et al., 2019; Saranya et al., 2022) limit the growth, composition, and regeneration capacity of mangrove stands (Gitau et al.2023), seagrass beds (Uku et al.,2021) and coral reefs in Diani-Chale and Kisite-Mpunguti marine parks (Obura et al.,2021). Unfortunately, natural heritage to include national forest reserves and sacred forests, known as *Kayas*, stand to lose 50% of cover by 2050 as a result of rapid arid landscape expansion (Parracciani et.al.,2023; Haile et al.,2020).

The Representative Concentration Pathway (RCP), used by the Intergovernmental Panel on Climate Change to describe future climate scenarios, denotes that global climate change will result in a 4 °C increase in temperature (Vincent et al., 2011; Palmer,2023) and a 20% variation in rainfall by 2100 (Nicholson, 2017; IPCC, 2021). In Kenya, General Circulation Models (GCMs) predict that mean annual temperatures will rise by 0.8°C to-1.5°C by 2030 (GoK, 2013) and 1.6°C to 2.7°C by 2060 (GoK, 2018). According to median climate models, temperatures will rise by 1.3 °C in 2030, 1.7 °C in 2050, and 2.2 °C in 2080 under the RCP6.0's medium/high emissions scenario (GIZ,2021; EPA,2022). In line with rising mean annual temperatures, the yearly number of very hot days, with daily maximum temperatures above 35 °C, is anticipated to rise by 25 in 2030, 36 in 2050, and 59 in 2080 (USAID, 2022). For instance, hot days on the northern Kenyan coast are anticipated to reach 300 per year by 2080 (Few et al., 2015; Gichangi et al., 2015).

Further, under RCP6.0, potential evapotranspiration is expected to rise by 1.9% in 2030, 3.0% in 2050 and 4.5% in 2080 (Gebrechorkos et al., 2019; World Bank Group, 2021). Unfortunately, prolonged drought cycles (Taylor et al., 2019; Painter et al., 2021) and recurring marine heat waves (Kairo, et al.,2021) result in biomass loss and ground aquifer depletion for instance at Ishakani, Kiunga, and Mambore in the northern Kenyan coast. As a result of frequent droughts in this region, historic sites such as Ashuwei, Sendeni, Mvindeni, and Rubu have been abandoned (Wilson, 2016). Overall, high temperatures are expected to worsen the state of surrounding Boni and Dondori forests, making fresh water supply even more unpredictable (Ongoma et.al.,2018; Lam et al., 2023).

Unfortunately, for most parts of the country, precipitation is expected to decrease by 8-10% between October and December, extending the hottest and driest months of January and February (Rowell et al.,2015; Wainwright et al.,2019). Additionally, under RCP6.0, the number of days with heavy precipitation will decrease from 9 in 2000 to 7 in 2080 (World Bank Group, 2021; USAID, 2022). With warmer sea surface temperatures, median climate models predict a sea-level rise of 10 cm by 2030, 21 cm by 2050, and 40 cm by 2080 (GIZ, 2021; Vousdoukas et al.,2022). Sea level rise and ENSO variability (Hansen, et al.,2019) are predicted to exacerbate erosion trends (Njiiri et al., 2024), beach loss (Omoumbo, 2013), and coastal upwelling (Mwakumanya, 2021). Reactive responses to rising sea levels are evidenced

by the need for construction and periodic maintenance of costly sea walls in historic settlements, such as Lamu Old Town (Figure 1) and Kizingitini (Figure 2) on Pate Island in the northern Kenya coast, respectively.

Heritage climatology emphasizes the need for detailed analysis on short-term pulses and long-term fluctuations in temperature and rainfall trends (Brimblecombe et al.,2024). The paper has sought to establish climate variability for the adaptation of maritime built heritage to climate change in the south Kenya coast. The goal is to provide a baseline for prioritizing conservation planning initiatives that improve capacity for dealing with climate change.

Figure 1: Sea wall, Lamu

Figure 2: Sea wall, Kizingitini.

Maritime Cultural and Natural Heritage in South Kenya Coast

Kwale County, a region that delimits the south Kenya coast, is located between 4.1816° S and 39.4606° E (Figure 3). The region is located in an Inter-Tropical Convergence Zone (ITCZ), which is an important component of the Earth's climate system (GoK, 2019). The timing of the short and long wet seasons is determined by two monsoon seasons: the Southwest monsoon, which occurs from April to June, and the Northeast monsoon, which occurs between October and April.

Maritime built heritage along the 120km littoral strip comprises of ancient mosques, tombs, wells, archaeology and historic buildings located in remote islands and fishing villages. Maritime natural heritage comprises Diani-Chale and Kisite-Mpunguti marine parks as well as 26 sacred forests, 24 of which are designated as national monuments and 2 are classified as UNESCO World Heritage Sites. Unfortunately, climate variability now limits the growth, composition, and regeneration capacity of mangroves (Kairo et al. 2021), and sacred forests known as *Kayas* (Jacobs et. al., 2021). Considering that erosion trends in the southern coast are three times higher than northern coast erosion trends (Njiiri,et.al.,2025), rising sea levels necessitate the need to erect higher plot boundaries and sea walls as observed for instance, at the periphery of Galu (Figure 4) and Gazi (Figure 5) historic ruins, respectively.

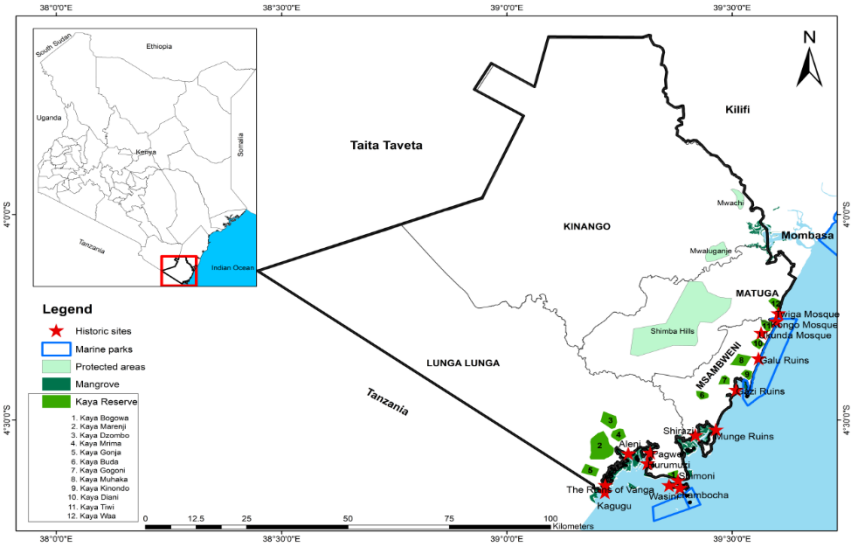

Figure 3: Kwale County, South Kenya Coast

Figure 4: Plot boundaries, Galu ruins

Figure 5: Sea walls, Gazi ruins.

For littoral historic sites, traditional building materials to include coral, timber, thatch, mud brick, wattle and daub are increasingly prone to bleaching, scaling, corrosion, exfoliation, sub/effloresce, detachment and collapse. The differential patterns of decay are observed for instance, at Kongo mosque on Tiwi beach, Diani (Figure 6) and the old British customs office in Vanga (Figure 7). Unfortunately, warmer air and sea surface temperatures contribute to the loss of familiar landscapes as evidenced by the spread of invasive plant species such as *Vachellia reficiens, Prosopis juliflora, Lantana camara, Azadirachta indica* and *Pedilianthus tithymaloides* (Betts et al., 2019; Cazalis et.al., 2022). Given that tourism is the main economic activity in the south Kenya coast, an analysis of climate trends warrants immediate attention considering that maritime cultural and natural heritage is at risk of irreversible loss.

Figure 6: Kongo Mosque, Diani

Figure 7: Old British Customs Office, Vanga

Methodology

The methodology described below was developed to better target climate adaptation in Kwale County, on Kenya's south coast. The goal was to provide a baseline for prioritizing conservation planning initiatives that improve capacity for dealing with climate change. To establish climate variability in the study area, climate data was sourced from the Kenya Meteorological Department (Table 1).

Table 1: Sources of Climate Data

Parameter	Data set	Variable	Source
Climate	Temperature (°C)	Average mean temperature Average minimum temperature Average maximum temperature	Kenya Meteorological Department (KMD)
	Rainfall (mm)	Average mean rainfall Average minimum rainfall Average maximum rainfall	

Data was analyzed using descriptive and inferential statistics, with means, standard deviations, coefficients of variance, and linear regressions calculated using the Statistical Package for Social Sciences (SPSS) version 23 to determine climate variability. The mean annual rainfall was estimated by dividing the average monthly rainfall for each year by the number of months (Equation 1).

Annual mean rainfall = ∑ Mean monthly rainfall / 12 (number of months) (Equation 1).

The mean annual temperature was calculated by dividing the average monthly temperature for each year by the number of months (Equation 2).

Annual mean temperature = ∑ Mean monthly temperature / 12 (number of months) (Equation 2).

To detect annual average rainfall and temperature variations across time, the data was run through SPSS chart builder to depict long term trends. Due to climate seasonality, missing monthly readings affected rainfall and temperature trend computations. As a result, annual averages were altered by extreme values.

For this reason, the standard deviation, a measure of the absolute dispersion of a dataset from its mean, was computed to aid in the comparison of data sets that shared similar means but with different ranges. The formula given in Equation 3 was used to calculate the standard deviation.

Standard deviation (S) = $\sqrt{\ \sum_{i=1}^{n} (x_i - \bar{x}) / n - 1}$ (Equation 3).

Where; $\sum$= Totality of individual values of $(x_i - \bar{x})$ for i - n (months), n = total sum of number of observations for 12 months, x_i = cumulative number of variables x, $\bar{x}$ = mean of variable x.

To expresses the standard deviation as a percentage of the mean, the coefficient of variation was computed to provide a relative measure of variability. While standard deviation is useful for understanding the data's spread in its original units (Schillaci and Schillaci, 2022), the coefficient of variance is essential for comparing variability across datasets with different scales or units, offering a standardized unit less comparison (Jalilibal et al., 2021; Santos and Dias, 2021). The formula given in Equation 4 was used to calculate coefficient of variance.

Coefficient of Variance = Standard deviation / Mean annual rainfall (Equation 4).

Further, a linear regression model was used to determine whether the dependent variable (rainfall or temperature) was a significant predictor of the independent variable (time). A 30-year timeframe from 1994 to 2024 was chosen based on the World Meteorological Organization's characterization of the timescale border between weather and climate (WMO,2020).

To calculate the proportion of variance in the data across the study period, R-squared of linear regression (R2), also known as coefficient of determination, was used. The coefficient indicates the degree of correlation between the independent and dependent variables (Arrieta-Pastrana et al., 2022; Tofu and Mengistu, 2022), in this case, selected climate data variables and time. Finally, an independent sample t-test was performed to determine whether there was a significant difference in average mean rainfall between the first and last two years. Similarly, the t-test method was used on average minimum and maximum temperatures to determine the statistical difference between the first and last two years.

Results and Interpretation

Table 2 shows the trend of average mean temperatures from 1994 to 2024, as calculated by descriptive statistics. The average monthly temperature's coefficient of variance (CV) exhibits low and high standard deviation (SD). February had the lowest CV of 0.013 and SD of 0.348 from the mean ($\bar{x}$=27.09), whereas April had the highest CV of 0.021 and SD of 0.541 from the mean ($\bar{x}$=25.58). Computed skewness, a measure of data asymmetry, ranges from -0.740 to 0.951, indicating a left-tailed (negative) distribution. The observed kurtosis readings show the highest kurtosis of 1.291 and the lowest kurtosis of -0.113 for the months of December and July. The platykurtic distribution, which has a flatter peak and narrower tails than a normal distribution, showed a minimal chance of severe outcomes in mean temperature for all months

Table 2: Average Mean Temperature for the year 1994 to 2024

	Jan	Feb	Mar	Apr	May	Jun	July	Aug	Sep	Oct	Nov	Dec
Average	26.72	27.09	26.87	25.58	24.45	23.60	22.96	22.97	23.58	24.41	25.21	26.05
Std Error	0.080	0.062	0.085	0.097	0.089	0.074	0.077	0.068	0.064	0.086	0.089	0.084
Median	26.81	27.06	26.77	25.58	24.51	23.56	22.94	22.98	23.60	24.43	25.21	26.06
SD	0.443	0.348	0.475	0.540	0.494	0.411	0.430	0.378	0.354	0.480	0.495	0.465
SV	0.196	0.121	0.225	0.292	0.244	0.169	0.185	0.143	0.125	0.230	0.245	0.216
Kurtosis	0.179	0.844	0.462	-0.399	-0.949	-0.696	-0.113	-0.495	-0.187	-0.772	0.959	1.291
Skewness	-0.696	0.501	0.951	0.360	0.095	0.145	0.474	0.158	0.395	0.180	0.633	-0.740
Range	1.954	1.656	1.920	2.139	1.784	1.539	1.762	1.566	1.484	1.736	2.226	2.208
Min	25.60	26.44	26.23	24.68	23.63	22.88	22.25	22.20	23.00	23.58	24.28	24.82
Max	27.55	28.10	28.15	26.82	25.42	24.42	24.01	23.77	24.48	25.32	26.51	27.02
CI (95%)	0.163	0.128	0.174	0.198	0.181	0.151	0.158	0.139	0.130	0.176	0.182	0.171
CV	0.017	0.013	0.018	0.021	0.020	0.017	0.019	0.016	0.015	0.020	0.020	0.018

SD: Standard deviation; Std E: Standard error; SV: Sample variance; CI: Coefficient of Interval; CV: Coefficient variance

The trend in average minimum temperatures from 1994 to 2024 was determined using statistical metrics of central tendency and dispersion (Table 3). April had the lowest CV of 0.019 and SD of 0.412 compared to the mean ($\bar{x}$=21.91). October showed the highest CV of 0.039 and SD of 0.765 from the mean ($\bar{x}$=19.68). Computed skewness ranges from -0.95 to 0.15, indicating a left-tailed (negative) distribution. The observed kurtosis readings show the highest kurtosis of 3.42 and the lowest kurtosis of -0.94 in September and November, respectively. The leptokurtic distribution predicted a higher chance of extreme outcomes in average minimum temperature for September.

Table 3: Average Minimum Temperature for the year 1994 to 2024

	Jan	Feb	Mar	Apr	May	Jun	July	Aug	Sep	Oct	Nov	Dec
Average	21.90	21.91	22.20	21.91	20.64	19.70	18.92	18.75	19.06	19.68	20.68	21.50
Std Error	0.103	0.115	0.094	0.074	0.087	0.075	0.080	0.104	0.113	0.137	0.121	0.078
Median	21.83	22.03	22.20	21.94	20.64	19.62	19.07	18.80	19.11	19.72	20.80	21.56
SD	0.573	0.640	0.526	0.412	0.485	0.419	0.445	0.578	0.630	0.765	0.676	0.434
SV	0.328	0.410	0.277	0.170	0.235	0.176	0.198	0.334	0.397	0.585	0.458	0.188
Kurtosis	0.592	1.048	0.500	-0.232	-0.870	-1.229	-0.630	0.879	3.425	2.441	-0.946	0.085
Skewness	0.155	-0.955	0.241	0.026	-0.239	0.026	-0.262	-0.802	-0.963	-1.153	-0.245	-0.373
Range	2.624	2.784	2.293	1.682	1.676	1.364	1.884	2.474	3.375	3.632	2.603	1.806
Min	20.66	20.24	21.11	21.09	19.75	18.96	17.92	17.20	16.94	17.27	19.26	20.57
Max	23.28	23.02	23.41	22.77	21.42	20.32	19.81	19.67	20.31	20.91	21.86	22.37
CI (95%)	0.210	0.235	0.193	0.151	0.178	0.154	0.163	0.212	0.231	0.280	0.248	0.159
CV	0.026	0.029	0.024	0.019	0.023	0.021	0.024	0.031	0.033	0.039	0.033	0.020

SD: Standard deviation; Std E: Standard error; SV: Sample variance; CI: Coefficient of Interval; CV

: Coefficient variance

The linear regression y=0.0276x - 34.901, R^2 = 0.613 shows an oscillating monotonic trend of average minimum temperature with fewer extremes recorded in 1996 and 1999, with low peaks of 19.8°C and 20°C, respectively (Figure 8). Across the trend, the climate variability anomaly peaked in 2015 and 2024, with higher temperatures reaching 21°C and 21.3°C, respectively. The average minimum temperature increased by +1.4°C during the course of 30 years, representing a 6.6% gain.

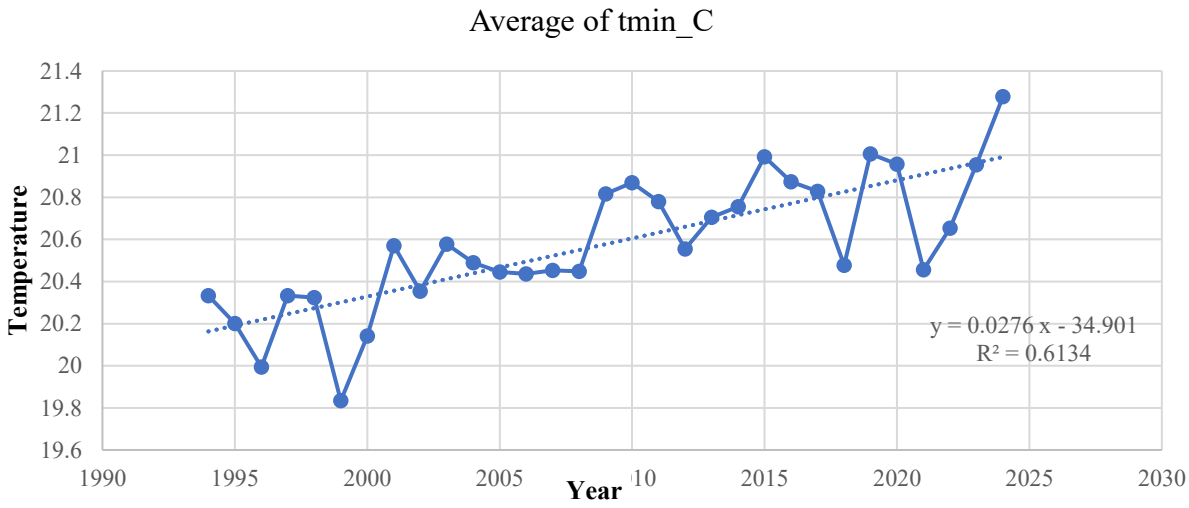

Figure 8: Average minimum temperature (1990-2024).

Table 4 shows the trend in average maximum temperatures from 1994 to 2024, as determined by descriptive statistics. June had the lowest CV of 0.37 and SD of 73.56 from the mean ($\bar{x}$ = 197.04), while January had the highest CV of 0.97 and SD of 55.06 from the mean ($\bar{x}$ = 56.67). The skewed values range from 0.11 to 2.55, indicating a typical distribution spread. Kurtosis readings ranged from -0.49 to 7.92. The leptokurtic distribution revealed a larger chance of extreme outcomes in average maximum temperatures in April and November, respectively.

Table 4: Average Maximum Temperature for the year 1994 to 202

	Jan	**Feb**	**Mar**	**Apr**	**May**	**Jun**	**Jul**	**Aug**	**Sep**	**Oct**	**Nov**	**Dec**
Average	56.7	34.0	121.7	349.8	457.6	197.4	142.	121.7	142.0	230.4	253.3	148.9
Std E	9.89	3.20	12.41	34.97	37.50	13.21	11.69	9.02	16.50	29.57	31.78	13.85
Median	32.1	28.9	103.8	301.8	454.6	195.4	125.7	118.5	127.3	182.1	197.6	126.1
SD	55.0	17.0	69.08	194.2	208.0	73.56	65.07	50.22	91.85	164.4	176.4	77.14
SV	3031	316.	4772.	37916	43596	5411.	4237	2522.	8435.	27107	31309	5950
Kurtosis	2.89	1.57	0.43	5.42	0.65	1.08	2.19	-0.49	-0.37	2.22	7.92	-1.06
Skewness	1.80	1.01	1.00	1.99	0.74	0.11	1.53	0.54	0.85	1.60	2.55	0.26
Range	2151	78.1	270.5	948.9	933.8	345.9	270.3	183.3	306.8	637.3	888.0	251.8
Min	11.5	10.3	36.26	127.1	98.87	40.31	71.13	50.89	36.15	65.59	67.75	31.30
Max	2208	89.4	307.1	1075.	1032.	386.2	341.5	234.5	342.8	703.2	956.1	283.2
CI (95%)	20.20	6.53	25.34	71.42	76.59	26.98	23.87	18.42	33.69	60.39	64.90	28.29
CV	0.97	0.51	0.57	0.56	0.46	0.37	0.46	0.41	0.64	0.71	0.70	0.52

SD: Standard deviation; Std E: Standard error; SV: Sample variance; CI: Coefficient of Interval; CV: Coefficient variance

The linear trend of average maximum temperature (Figure 9) is monotonic (y=0.0311x + 31.13, R^2=0.396). The highest maximum temperatures were recorded in 2012 and 2024, when the average maximum temperature rose to 32.10°C and 32.40°C, respectively. Overall, the average maximum temperature increased by +1.7°C during 30 years, representing a 5.2% gain. Since the pre-industrial period, the earth's surface temperature has increased by 1°C. Furthermore, according to an IPCC (2018) report, the earth's temperature will rise by 1.5 degrees Celsius by 2030. Thus, local patterns in average maximum temperature support the global average warming index, as does the occurrence of recurring marine heat waves along the southern coastline.

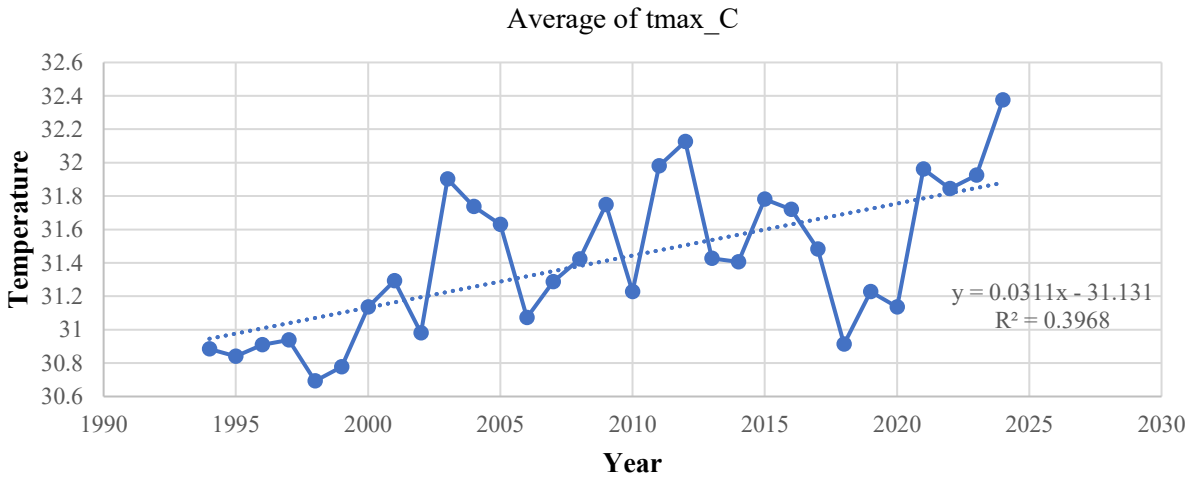

Figure 9: Average maximum temperature (1990-2024)

Table 5 shows the trend in average mean rainfall from 1994 to 2024, as determined by descriptive statistics. The coefficient of variance (CV) of average monthly rainfall reveals both low and high standard deviation (SD). August had the lowest CV of 0.301 and lowest SD of 15.14 from the mean ($\bar{x}$=50.37), whereas January had the greatest CV of 1.148 and SD of 35.13 from the mean ($\bar{x}$=30.61). Computed skewness, a measure of data asymmetry, ranges from -0.352 to 2.538, indicating a right-tailed (positive) distribution. Kurtosis readings show a maximum of 9.492 in February and a minimum of -0.003 in September. The leptokurtic distribution revealed a higher chance of extreme outcomes in average mean rainfall for January, February, April, October, and November.

Table 5:

Table 5: Average Mean Rainfall for the year 1994 to 2024

	Jan	**Feb**	**Mar**	**Apr**	**May**	**Jun**	**July**	**Aug**	**Sep**	**Oct**	**Nov**	**Dec**
Average	30.6	16.84	73.15	166.2	192.4	69.90	57.27	50.37	50.57	116.0	151.4	92.28
Std Error	6.31	1.798	7.828	14.72	13.71	3.960	4.044	2.720	4.312	16.26	16.60	9.273
Median	14.9	14.61	62.38	145.0	195.8	75.30	51.94	48.60	43.66	84.82	125.0	80.13
SD	35.1	10.01	43.58	81.85	76.39	22.04	22.51	15.14	24.00	90.45	92.42	51.62
SV	1234.63	100.264	1899.576	6700.391	5836.543	486.115	506.925	229.323	576.287	8181.959	8542.145	2665.556
Kurtosis	6.27	9.492	-0.262	3.753	-0.088	0.097	2.333	1.273	-0.003	3.836	8.717	-1.217
Skewness	2.37	2.587	0.808	1.705	0.269	-0.352	1.351	1.084	0.842	1.903	2.538	0.373
Range	157.	51.65	153.6	382.8	311.2	96.48	107.7	65.91	89.23	386.3	487.2	165.0
Min	4.29	6.943	19.77	68.91	49.06	19.68	21.83	29.95	18.79	30.33	41.79	18.19
Max	161.	58.59	173.4	451.7	360.5	116.1	129.6	95.83	108.0	416.6	528.9	183.2
CI (95%)	12.8	3.673	15.98	30.02	28.02	8.087	8.259	5.555	8.805	33.17	33.90	18.93
CV	1.14	0.594	0.596	0.492	0.397	0.315	0.393	0.301	0.475	0.779	0.610	0.559

SD: Standard deviation; Std E: Standard error; SV: Sample variance; CI: Coefficient of Interval; CV: Coefficient variance

The linear trend of the mean rainfall, y=4.99x -8957.6, R^2 = 0.00275 (Figure 10), revealed high precipitation anomalies in the years 1996, 2018, and 2023, with rainfall levels of 1600mm, 1500mm, and 1600mm, respectively. Despite peak precipitation anomalies, precipitation was shown to gradually increase during the trend. Thus, linear regressions on average maximum and minimum rainfall were required to reveal variability for the March-April-May (MAM) long rainy season and the October-November-December (OND) short rainy season, respectively.

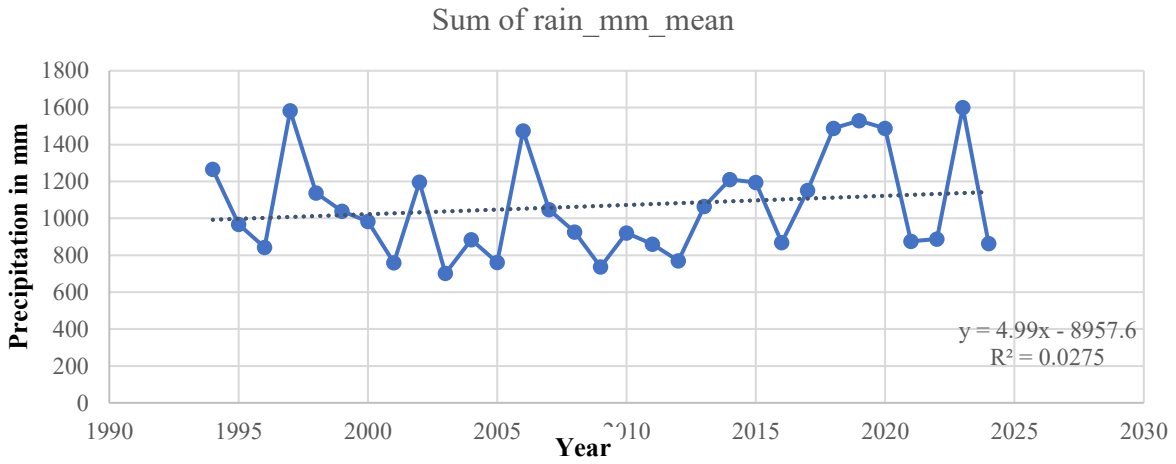

Figure 10: Figure 10: Average mean rainfall (1990-2024)

The trend of average minimum rainfall between 1994 and 2024 was evaluated using statistical metrics of central tendency and dispersion (Table 6). August had the lowest CV of 0.27 and SD of 4.87 compared to the mean ($\bar{x}$=17.90). January showed the greatest CV of 1.60 and SD of 18.84 from the mean ($\bar{x}$=11.80). Computed skewness ranges from 0.01 to 2.99, indicating that the distribution was strongly skewed. The observed kurtosis values show the highest kurtosis of 10.63 and the lowest kurtosis of -0.64 for the months of January and May. The leptokurtic distribution showed a higher likelihood of extreme outcomes in average minimum rainfall in January, February, and November.

Table 6: Average Minimum Rainfall for the year 1994 to 2024

	Jan	Feb	Mar	Apr	May	Jun	Jul	Aug	Sep	Oct	Nov	Dec
Average	11.80	5.62	37.70	70.48	49.05	21.86	17.28	17.90	16.45	35.12	88.06	46.91
Std Error	3.38	1.11	4.83	6.67	3.21	1.27	0.87	0.88	1.23	5.12	9.47	5.28
Median	6.54	6.13	32.64	58.89	49.29	21.20	16.06	16.32	15.47	26.60	73.96	35.00
SD	18.84	6.21	26.87	37.11	17.87	7.05	4.85	4.87	6.84	28.52	52.72	29.38
SV	355.4	38.53	721.8	1377.	319.1	49.73	23.57	23.74	46.81	813.2	2773	863.5
Kurtosis	10.63	8.68	2.23	0.52	-0.64	-0.30	0.32	2.70	0.73	1.93	6.03	-0.35
Skewness	2.99	2.29	1.41	1.18	0.17	0.01	0.45	1.72	0.98	1.64	2.26	0.80
Range	91.48	31.10	116.1	137.6	67.01	29.20	22.40	19.63	28.17	107.0	259.3	105.7
Min	0.00	0.00	8.00	27.00	15.18	7.35	6.81	12.57	6.82	8.53	22.98	8.69
Max	91.48	31.10	124.1	164.1	82.19	36.55	29.21	32.20	34.99	116.3	282.1	114.3
CI (95%)	6.91	2.28	9.86	13.61	6.55	2.59	1.78	1.79	2.51	10.46	19.34	10.78
CV	1.60	1.10	0.71	0.53	0.36	0.32	0.28	0.27	0.42	0.81	0.60	0.63

SD: Standard deviation; Std E: Standard error; SV: Sample variance; CI: Coefficient of Interval; CV: Coefficient variance

The linear trend of average minimum rainfall shows an oscillating tendency, y=0.101x + 168.34, R^2=0.0079, with precipitation extremes ranging from 50mm to 60mm in 2006 and 2023, respectively (Figure 11). Across the trend, the average minimum rainfall anomaly reached its lowest point in 2009 and 2011, with precipitation quantities of 19mm and 20mm, respectively. Overall, the average minimum rainfall increased by 41mm during 30 years, representing a 68% rise.

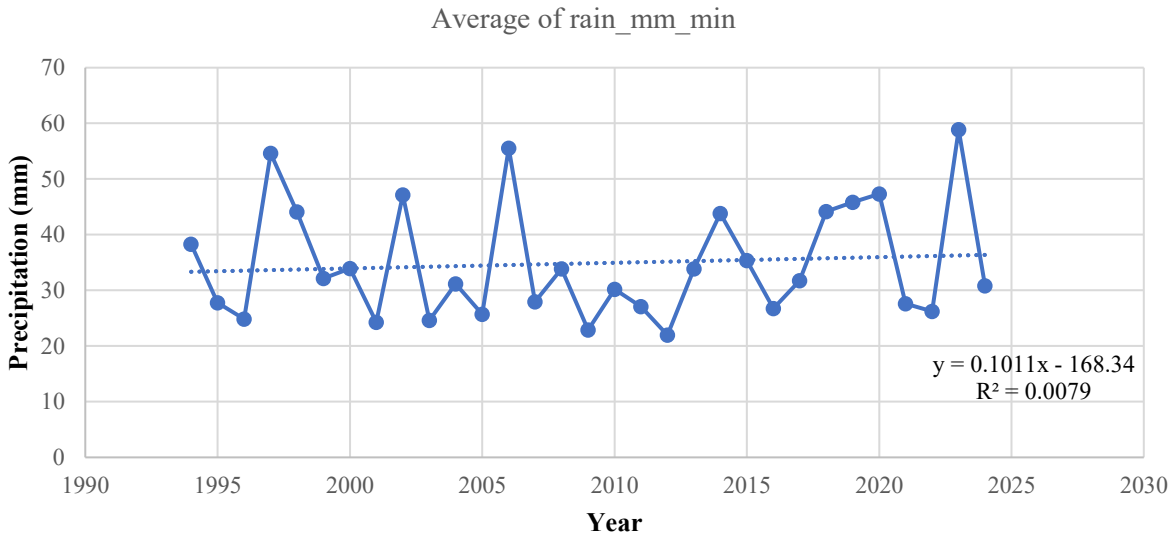

Figure 11: Average minimum rainfall (1990-2024)

Table 7 shows the evolution of average maximum rainfall from 1994 to 2024 based on descriptive statistics. July had the lowest CV of 0.0019 and SD of 0.54 compared to the mean ($\bar{x}$=28.43). October showed the highest CV of 0.034 and SD of 1.70 from the mean ($\bar{x}$=31.18). Computed skewness ranges from -0.62 to 1.31, indicating a left-skewed (negative) distribution. The observed kurtosis readings show the highest kurtosis of 2.54 and the lowest kurtosis of -0.81 for the months of November and September. The leptokurtic distribution showed a higher chance of extreme outcomes in average maximum rainfall in November.

Table 7: Average minimum rainfall (1990-2024)

	Jan	Feb	Mar	April	May	June	July	Aug	Sep	Oct	Nov	Dec
Average	34.27	35.18	34.40	31.72	30.01	28.88	28.43	28.79	29.77	31.18	31.6	32.6
Std Error	0.182	0.161	0.160	0.200	0.162	0.112	0.098	0.114	0.133	0.192	0.15	0.14
Median	34.30	35.22	34.50	31.58	30.06	28.92	28.40	28.84	29.66	31.33	31.4	32.5
SD	1.013	0.894	0.893	1.113	0.901	0.623	0.544	0.637	0.742	1.069	0.85	0.81
SV	1.026	0.800	0.798	1.240	0.811	0.389	0.296	0.406	0.551	1.143	0.72	0.66
Kurtosis	0.176	1.128	-0.225	-0.466	-0.669	-0.525	-0.494	-0.498	-0.809	-0.680	2.54	1.16
Skewness	-0.622	-0.134	-0.418	0.320	0.126	0.050	0.250	-0.193	0.180	-0.204	1.31	0.29
Range	3.994	4.399	3.593	4.554	3.235	2.354	2.009	2.607	2.782	4.022	3.95	3.82
Min	31.97	33.07	32.20	29.82	28.50	27.74	27.57	27.47	28.41	29.23	30.3	30.8
Max	35.96	37.47	35.85	34.44	31.82	30.05	29.51	30.09	31.19	33.24	34.2	34.7
CI (95%)	0.371	0.328	0.328	0.408	0.330	0.229	0.200	0.234	0.272	0.392	0.31	0.29
CV	0.030	0.025	0.026	0.035	0.030	0.022	0.019	0.022	0.025	0.034	0.027	0.025

SD: Standard deviation; Std E: Standard error; SV: Sample variance; CI: Coefficient of Interval; CV: Coefficient variance

The linear trend of average maximum rainfall shows an oscillating tendency, y=1.7109x - 3249.1, R^2=0.0916, with precipitation extremes ranging from 250mm to 300mm in 1997 and 2020, respectively (Figure 12). Across the trend, the average maximum rainfall anomaly reached its lowest point in 2003 and 2008, with precipitation totals of 110mm and 125mm. Overall, the combined increase in average maximum rainfall was 190mm, a 62% increase over 30 years.

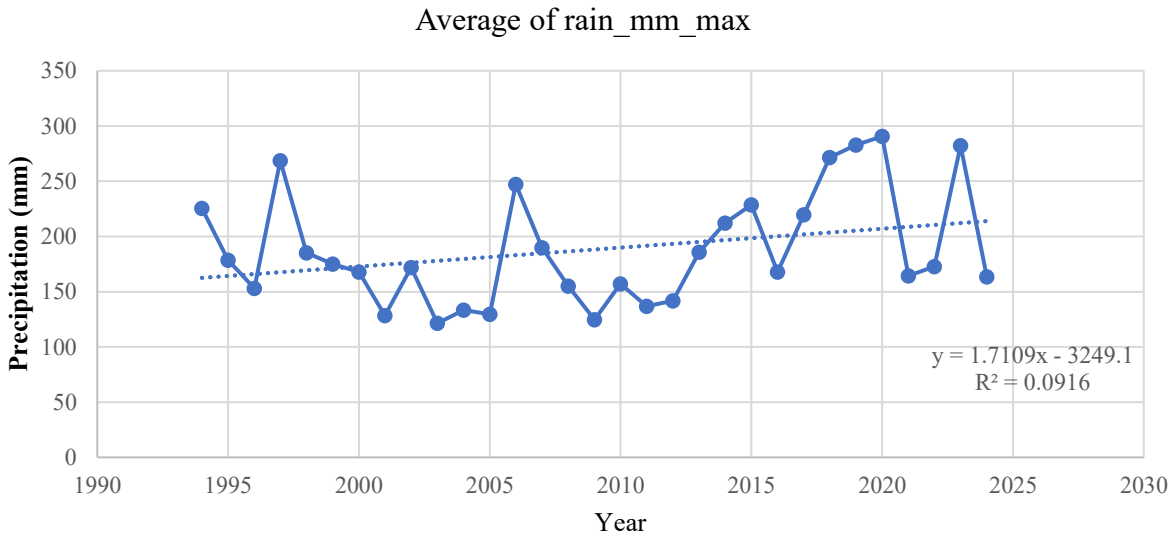

Figure 12: Average maximum rainfall (1990-2024).

A paired t-test was performed on meteorological data to determine whether there was a significant variance in rainfall and temperature during the study period. The data was divided into two sets: the first set contained measurements collected in the first two years (1994 and 1995), while the second set contained measurements obtained in the last two years (2023 and 2024). The first test was conducted to determine the difference in mean yearly rainfall between the first and last two years. The presumption was that rainfall levels in the latter two years had been much lower than in the first two years of data collection.

The results of the rainfall variability t-tests (Table 8) reveal that the average rainfall for the first two years was considerably lower than that of the last two years (t (-0.525,1.000) = 6.3138, P =0.3460). This suggests that mean annual rainfall is gradually increasing throughout the southern coast.

Table 8: Mean annual rainfall T-Test

	Mean Annual Rainfall 1994-1995	**Mean Annual Rainfall 2023-2024**
Mean	93.0884	102.6537
Variance	310.8979	1881.4109
Observations	2.0000	2.0000
Pearson Correlation	1.0000	
Hypothesized Mean Difference	0.0000	
Df	1.0000	
t Stat	-0.5255	
P(T<=t) one-tail	0.3460	
t Critical one-tail	6.3138	
P(T<=t) two-tail	0.6920	
t Critical two-tail	12.7062	

Prior analysis revealed that the average maximum temperature in the study area had risen by 1.6°C over 30 years. The mean maximum temperature of the first and last two years was compared using the previously indicated t-test method (Table 9). Based on the findings, it is clear that the maximum temperature over the recent two years is considerably greater than the temperature over the previous two years (t (-5.2086, 1.0000) = 6.3138, P=0.0604).

Table 9: Average Maximum Temperature T-Test

	Average Max temp 1994-1995	**Average Max temp 2023-2024**
Mean	30.8624	32.1500
Variance	0.0009	0.1017
Observations	2.0000	2.0000
Pearson Correlation	-1.0000	
Hypothesized Mean Difference	0.0000	
Df	1.0000	
t Stat	-5.2086	
P(T<=t) one-tail	0.0604	
t Critical one-tail	6.3138	
P(T<=t) two-tail	0.1208	

t Critical two-tail	12.7062	

Similarly, the average minimum temperature was analysed to determine whether there was a difference between the first and last two years, with the results displayed in Table 10. The data reveal that the average minimum temperature over the last two years is considerably higher than in the first two years (t (--3.7226, 1.0000) = 6.3138, P=0.0835).

Table 10: Average Minimum Temperature T-Test

	Average Min temp 1994-1995	**Average Min temp 2023-2024**
Mean	20.2667	21.1160
Variance	0.0088	0.0524
Observations	2.0000	2.0000
Pearson Correlation	-1.0000	
Hypothesized Mean Difference	0.0000	
Df	1.0000	
t Stat	-3.7226	
P(T<=t) one-tail	0.0835	
t Critical one-tail	6.3138	
P(T<=t) two-tail	0.1671	
t Critical two-tail	12.7062	

Conclusion

The paper sought to establish climate trends to better target climate adaptation for maritime cultural and natural heritage in the south Kenya coast. The study concludes that climate variability is significant in the study area. In 30 years, average maximum and minimum temperatures increased by1.7 °C and 1.4°C, respectively, indicating hotter and colder cycles. The cumulative increase in average maximum and minimum rainfall was 190mm and 19mm, representing a 62% and 68% increase over 30 years, respectively. However, the low values of 600 mm of average mean rainfall recorded in the month of February and the high quantities of 1600 mm recorded in May, fluctuate more between the 2015 to 2025 decade than the 2005 to 2015 and 1995 to 2005 decades, demonstrating greater unpredictability in rainfall patterns.

Overall, the unpredictability of short and long rainy seasons has increased during the last ten years compared to the previous twenty. Furthermore, low R-square values have statistically significant coefficients, indicating great variability around the regression line. Thus, smaller intervals are required when presenting future climate trends for the long and short rainy seasons. Nonetheless, the need for climate-sensitive adaptation measures is urgent, given that maritime cultural and natural heritage is under threat from unprecedented climate change.

Recommendations

The Paris Agreement calls for the assessment of climate change impacts with a view to formulate holistic actions geared towards climate adaptation. On the policy front, Kenya has formulated policies on climate change to include: The Climate Change Response Strategy 2010; the National Climate Change Framework

Policy of 2016; the National Adaptation Plan 2015-2030 and National Climate Change Action Plan 2020. All these policies have since been enacted into law under the Climate Change Act of 2016. However, coastal counties are yet to mainstream these climate change actions into adaptation and heritage planning processes. To aid conservators, curators and urban planners in the adaptation of maritime heritage to climate change, the paper recommends the following actions:

- Map erosion hotspots and flood zones.
- Monitor salt crystallization and cracks.
- Apply salt-resistant mortars and plasters.
- Apply anti-corrosion treatments for metals.
- Improve site drainage and capillary breaks.
- Adjust setbacks to protect sites from erosion.
- Restrict anchoring to stabilize sea grass beds.
- Control land use to safeguard forest ecosystems.
- Stabilize and consolidate low lying historic sites.
- Preserve salt marshes to reduce high wave action.
- Restore mangroves to reduce saltwater intrusion.

Disclosure Statement

The authors report that there are no competing interests to declare.

Funding Details

No funding was received for this study.

References

Arrieta-Pastrana, A., Saba, M., & Alcázar, A. P. (2022). Analysis of climate variability in a time series of precipitation and temperature data: A case study in Cartagena de Indias, Colombia. *Water, 14*(9), 1378. https://doi.org/10.3390/w14091378

Betts, J., Young, R. P., Hilton-Taylor, C., Hoffmann, M., Rodríguez, J. P., Stuart, S. N., & Milner-Gulland, E. J. (2019). A framework for evaluating the impact of the IUCN Red List of threatened species. *Conservation Biology, 34*(3), 632–643. https://doi.org/10.1111/cobi.13454

Brimblecombe, P., & Richards, J. (2024). Applied climatology for heritage. *Theoretical and Applied Climatology, 155*(8), 7325–7333. https://doi.org/10.1007/s00704-024-05059-6

Cazalis, V., Di Marco, M., Butchart, S. H. M., Akçakaya, H. R., González-Suárez, M., Meyer, C., et al. (2022). Bridging the research–implementation gap in IUCN Red List assessments. *Trends in Ecology & Evolution, 37*(4), 359–370. https://doi.org/10.1016/j.tree.2021.12.002

Environmental Protection Agency. (2022). *Climate change indicators: Seasonal temperature*. United States Environmental Protection Agency. https://www.epa.gov/climate-indicators/climate-change-indicators-seasonal-temperature

Few, R., Satyal, P., McGahey, D., Leavy, J., Budds, J., Assen, M., … Bewket, W. (2015). *Vulnerability and adaptation to climate change in the semi-arid regions of East Africa*. Ottawa.

Gebrechorkos, S. H., Hülsmann, S., & Bernhofer, C. (2019). Long-term trends in rainfall and temperature using high-resolution climate datasets in East Africa. *Scientific Reports, 9*, 11376.

Gichangi, E. M., Gatheru, M., Njiru, E. N., Mungube, E. O., Wambua, J. M., & Wamuongo, J. W. (2015). Assessment of climate variability and change in semi-arid eastern Kenya. *Climatic Change, 130*(2), 287–297. https://doi.org/10.1007/s10584-015-1341-2

Gitau, P. N., Duvail, S., & Verschuren, D. (2023). Evaluating the combined impacts of hydrological change, coastal dynamics and human activity on mangrove cover and health in the Tana River Delta, Kenya. *Regional Studies in Marine Science, 61*, 102898. https://doi.org/10.1016/j.rsma.2023.102898

GIZ. (2021). *Climate risk profile: Kenya*. German Corporation for International Cooperation.

Government of Kenya. (2013). *National Climate Change Action Plan (NCCAP) 2007–2013*. Government Press.

Government of Kenya. (2018). *National Climate Change Action Plan (Kenya): 2018–2022*. Ministry of Environment and Forestry.

Government of Kenya. (2019). *Integrated coastal zone action plan for Kenya (2019–2023)*. National Environment Management Authority.

Haile, G. G., Tang, Q., Hosseini-Moghari, S., Liu, X., Gebremicael, T. G., Leng, G., Kebede, A., Xu, X., & Yun, X. (2020). Projected impacts of climate change on drought patterns over East Africa. *Earth's Future, 8*(7). https://doi.org/10.1029/2020EF001502

Hansen, J., Satoa, M., Ruedy, R., Schmidt, G. A., & Lo, K. (2019). *Global temperature in 2018 and beyond*. Earth Institute, Columbia University.

Intergovernmental Panel on Climate Change. (2018). *Global warming of 1.5°C: Summary for policymakers*. World Meteorological Organization.

Intergovernmental Panel on Climate Change. (2021). *Climate change 2021: The physical science basis*. Cambridge University Press.

Jacobs, Z. L., Yool, A., Jebri, F., Srokosz, M., Van Gennip, S., Kelly, S. J., et al. (2021). Key climate change stressors of marine ecosystems along the path of the East African coastal current. *Ocean & Coastal Management, 208*, 105627. https://doi.org/10.1016/j.ocecoaman.2021.105627

Jalilibal, Z., Amiri, A., Castagliola, P., & Khoo, M. B. (2021). Monitoring the coefficient of variation: A literature review. *Computers & Industrial Engineering, 161*, 107600. https://doi.org/10.1016/j.cie.2021.107600

Kairo, J., Mbatha, A., Murithi, M. M., & Mungai, F. (2021). Total ecosystem carbon stocks of mangroves in Lamu, Kenya, and their potential contributions to the climate change agenda in the country. *Frontiers in Forests and Global Change, 4*. https://doi.org/10.3389/ffgc.2021.709227

Kazungu, K. (2024, August 31). Concerns raised over frequent destruction of coast seawalls. *The Nation*.

Lam, M. R., Matanó, A., Van Loon, A. F., Odongo, R. A., Teklesadik, A. D., Wamucii, C. N., Van Den Homberg, M. J. C., Waruru, S., & Teuling, A. J. (2023). Linking reported drought impacts with drought indices, water scarcity and aridity: The case of Kenya. *Natural Hazards and Earth System Sciences, 23*(9), 2915–2936. https://doi.org/10.5194/nhess-23-2915-2023

Lyon, B., & Vigaud, N. (2017). Unraveling East Africa's climate paradox. *Geophysical Monograph*, 265–281. https://doi.org/10.1002/9781119068020.ch16

Maina, J. M., Bosire, J. O., Kairo, J. G., Bandeira, S. O., Mangora, M. M., Macamo, C., Ralison, H., & Majambo, G. (2021). Identifying global and local drivers of change in mangrove cover and the implications for management. *Global Ecology and Biogeography, 30*(10), 2057–2069. https://doi.org/10.1111/geb.13368

Mulonga, J., & Olago, D. (2023). Perceptions of climate variability and change in coastal Kenya: The case of mangrove-dependent communities in the Lower Tana Delta. *Environmental Challenges, 13*, 100799. https://doi.org/10.1016/j.envc.2023.100799

Mwakumanya, M. A. (2021). Beach erosion hazard vulnerability assessment of Bamburi Beach in Mombasa, Kenya. *International Journal of Environmental Science and Development, 12*(3), 80–86. https://doi.org/10.18178/ijesd.2021.12.3.1322

Nicholson, S. E. (2017). Climate and climate variability of rainfall over Eastern Africa. *Reviews of Geophysics, 55*(3), 590–635.

Njiiri, W., Njuguna, M., & Wahome, E. (2024). Determination of shoreline variability for adaptation of maritime built heritage to climate change: A case of Southern Kenya Coast. *The Historic Environment: Policy & Practice*, 1–17. https://doi.org/10.1080/17567505.2024.2435083

Njiiri, W., Njuguna, M., & Wahome, E. (2025). Establishing historical shoreline trends for adaption of maritime built heritage to climate change, Part 2: The Northern Kenya Coast. *The Historic Environment: Policy & Practice*, 1–20. https://doi.org/10.1080/17567505.2025.2470475

Obura, D., Gudka, M., Samoilys, M., Osuka, K., Mbugua, J., Keith, D. A., et al. (2021). Vulnerability to collapse of coral reef ecosystems in the Western Indian Ocean. *Nature Sustainability, 5*(2), 104–113. https://doi.org/10.1038/s41893-021-00817-0

Oliver, E. C. J., Burrows, M. T., Donat, M. G., Gupta, A. S., Alexander, L. V., Perkins-Kirkpatrick, S. E., et al. (2019). Projected marine heatwaves in the 21st century and the potential for ecological impact. *Frontiers in Marine Science, 6*. https://doi.org/10.3389/fmars.2019.00734

Omuombo, C. A., Olago, D. O., & Odada, E. O. (2013). Coastal erosion. In *Developments in earth surface processes* (pp. 331–339). https://doi.org/10.1016/B978-0-444-59559-1.00022-0

Ongoma, V., Chen, H., & Omony, G. W. (2018). Variability of extreme weather events over the equatorial East Africa: A case study of rainfall in Kenya and Uganda. *Theoretical and Applied Climatology, 131*(1–2), 295–308. https://doi.org/10.1007/s00704-016-1973-9

Painter, S. C., Popova, E., & Roberts, M. J. (2021). An introduction to East African Coastal Current ecosystems: At the frontier of climate change and food security. *Ocean & Coastal Management, 216*, 105977. https://doi.org/10.1016/j.ocecoaman.2021.105977

Palmer, P. I., Wainwright, C. M., Dong, B., Maidment, R. I., Wheeler, K. G., Gedney, N., et al. (2023). Drivers and impacts of Eastern African rainfall variability. *Nature Reviews Earth & Environment, 4*(4), 254–270. https://doi.org/10.1038/s43017-023-00397-x

Parracciani, C., Buitenwerf, R., & Svenning, J.-C. (2023). Impacts of climate change on vegetation in Kenya: Future projections and implications for protected areas. *Land, 12*(11), 2052. https://doi.org/10.3390/land12112052

Rowell, D. P., Booth, B. B. B., Nicholson, S. E., & Good, P. (2015). Reconciling past and future rainfall trends over East Africa. *Journal of Climate, 28*(24), 9768–9788. https://doi.org/10.1175/JCLI-D-15-0140.1

Saranya, J. S., Roxy, M. K., Dasgupta, P., & Anand, A. (2022). Genesis and trends in marine heatwaves over the tropical Indian Ocean and their interaction with the Indian summer monsoon. *Journal of Geophysical Research: Oceans, 127*(2). https://doi.org/10.1029/2021JC017427

Schillaci, M. A., & Schillaci, M. E. (2022). Estimating the population variance, standard deviation, and coefficient of variation: Sample size and accuracy. *Journal of Human Evolution, 171*, 103230. https://doi.org/10.1016/j.jhevol.2022.103230

Taylor, S. F. W., Roberts, M. J., Milligan, B., & Ncwadi, R. (2019). Measurement and implications of marine food security in the Western Indian Ocean: An impending crisis? *Food Security, 11*(6), 1395–1415. https://doi.org/10.1007/s12571-019-00971-6

Tofu, D. A., & Mengistu, M. (2022). Observed time series trend analysis of climate variability and smallholder adoption of new agricultural technologies in West Shewa, Ethiopia. *Scientific African, 19*, e01448. https://doi.org/10.1016/j.sciaf.2022.e01448

Uku, J., Daudi, L., Alati, V., Nzioka, A., & Muthama, C. (2021). The status of seagrass beds in the coastal county of Lamu, Kenya. *Aquatic Ecosystem Health & Management, 24*(1), 35–42. https://doi.org/10.14321/aehm.024.01.07

USAID. (2022). *Kenya climate change country profile*.

Vincent, L. A., Aguilar, E., Saindou, M., Hassane, A. F., Jumaux, G., Roy, D., et al. (2011). Observed trends in indices of daily and extreme temperature and precipitation for the countries of the western Indian Ocean, 1961–2008. *Journal of Geophysical Research: Atmospheres, 116*(D10). https://doi.org/10.1029/2010JD015303

Vousdoukas, M. I., Clarke, J., Ranasinghe, R., Reimann, L., Khalaf, N., Duong, T. M., et al. (2022). African heritage sites threatened as sea-level rise accelerates. *Nature Climate Change, 12*(3), 256–262. https://doi.org/10.1038/s41558-022-01280-1

Wainwright, C. M., Marsham, J. H., Keane, R. J., Rowell, D. P., Finney, D. L., Black, E., & Allan, R. P. (2019). Eastern African paradox rainfall decline due to shorter, not less intense, long rains. *NPJ Climate and Atmospheric Science, 2*(1). https://doi.org/10.1038/s41612-019-0091-7

Wilson, T. H. (1980). *The monumental architecture and archaeology of the central and southern Kenya Coast*. National Museums of Kenya.

World Meteorological Organization. (2020). *State of the climate in Africa 2019* (WMO-No. 1253).

World Bank Group. (2021). *Climate risk country profile: Kenya*. World Bank Group